Materials Horizons

ROYAL SOCIETY OF CHEMISTRY

COMMUNICATION

View Article Online
View Journal | View Issue

Cite this: *Mater. Horiz.*, 2025, **12**, 9125

Received 13th May 2025,
Accepted 23rd July 2025

DOI: 10.1039/d5mh00911a

rsc.li/materials-horizons

Textile-integrated multilayer liquid metal soft circuits for multienvironment wearable electronics†

Brittan T. Wilcox,‡[a] Ella T. Williams‡[a] and Michael D. Bartlett *[ab]

Soft devices that are rugged yet deformable are essential for wearable technologies that perform in diverse environments. For textile-based wearable electronics, creating robust mechanical and electrical interconnections between electronic components on complex, deformable surfaces like textiles remains a central challenge. In this work, we present a scheme for the creation of textile electronics through multilayer liquid metal (LM) soft circuits, including robust integration with textiles and water resistance. The fabrication method enables multilayer construction with vertical interconnect access or vias, as well as the integration of rigid electronic components, to enable advanced electrical functionality while maintaining flexibility and stretchability. We achieve robust interlayer adhesion (up to 11 000 J m^{-2}) within the soft circuits by combining multiple soft welding processes. Furthermore, the influence of textile integration on electromechanical performance is determined, providing mechanistic guidance to enable textile-integrated LM soft circuits that stretch to 300% strain with resilience against environmental damage, including water resistance. These textile-based soft circuits enable sensing and data transfer, which we show through several examples including a distributed wearable camera system. This process is adaptable to a wide variety of circuit designs and layouts, providing a path forward for robust, textile integrated electronics.

New concepts

We introduce a new approach for creating textile-integrated, multilayer liquid metal (LM) soft circuits that combines high flexibility with advanced electrical functionality and environmental resilience. Integrating multilayer architectures and rigid components into wearable electronic textiles is challenging, and our method enables robust vertical interconnects through vias, strong interlayer adhesion (up to 11 000 J m^{-2}) through synergistic soft welding techniques, and compatibility with surface-mounted components within a fully stretchable, textile-conformable platform. Furthermore, new mechanistic guidance is provided for designing interlayer adhesion of wearable multilayer circuits, for the structure–mechanics–functionality relationship between textile, elastomer and liquid metal, especially regarding electromechanical properties of stretchable liquid metal conductors, and for the performance of such soft circuits in aqueous environments. The utility of these wearable electronics is demonstrated through several different devices including a wearable multi-camera system that delivers a simulated bird's-eye view, offering users an expanded, immersive awareness of their surroundings. This strategy advances the field by bridging soft electronics and textile-based systems, offering a robust and adaptable foundation for next-generation wearable devices.

Introduction

Creating robust interconnections between multiple electronic components across complex surfaces like textiles is a key challenge in developing advanced wearable electronics and sensor networks. Previous schemes to integrate conductive circuit materials with textiles have included encapsulating rigid printed circuit boards (PCB) on textiles with hot melt resins,[1] conductive threads woven into textiles,[2–5] mask-printing directly onto textiles,[6] iron-on conductive traces,[7,8] and copper lithography encapsulated in elastomer-embedded textiles.[9] Textile-integrated multilayer soft circuits offer a promising route to enhance wearable electronics by providing greater interconnect flexibility and mechanical conformability. Beyond flexibility, ensuring reliable operation in challenging environments is essential for the development of robust, next-generation wearables. Soft circuits are well suited to meet these demands, as they combine environmental and damage resilience with the ability to stretch and conform to complex, dynamic surfaces.

Emergent materials such as liquid metals (LM) have enabled soft circuits with new properties including extensibility, conformability, and self-healing,[10–16] and these materials have been used in different types of soft electronics.[17–26] Recently,

[a] *Mechanical Engineering, Soft Materials and Structures Lab, Virginia Tech, Blacksburg, VA 24061, USA. E-mail: mbartlett@vt.edu*
[b] *Macromolecules Innovation Institute, Virginia Tech, Blacksburg, VA 24061, USA*

† Electronic supplementary information (ESI) available. See DOI: https://doi.org/10.1039/d5mh00911a

‡ These authors contributed equally to this work.

electronic functions with increasing complexity have been enabled through new fabrication techniques that allow for multilayer LM soft circuits. The inclusion of vertical interconnect access (vias), which provide electrical connections between separate layers of a circuit, allows for greater circuit design complexity.[27] While rigid PCBs typically use drilled holes for vias, soft circuits have found alternative methods by using laser ablation,[28–31] lift-off patterning,[32] or selective stratification of LM droplets in a composite.[33] The integration of LM soft circuits into textiles has also provided a platform for wearable electronics,[14,34–38] bringing LM soft circuits farther into the forefront of next-generation devices. However, a comprehensive understanding of textile integration—including interlayer adhesion, the influence of textile substrates on electromechanical performance, and device durability in challenging environments—remains incomplete, yet is essential for advancing the field.

Creating wearables that withstand both user interaction and environmental stresses is essential for expanding their functionality and reliability in real-world applications.[39–43] For example, integration of water-resistant, soft, and stretchable circuits into underwater suits could enable new functionalities and ergonomic designs for underwater wearable electronics.[36,44–48] This is especially compelling when multilayer circuit architectures, enabled by vias, can be combined with rigid electronic components to form hybrid systems that maintain flexibility while enhancing capability. Despite their promise, the performance of LM soft circuits under harsh conditions, particularly full water submersion, remains underexplored. However, such conditions present a valuable opportunity, as soft circuits offer inherent advantages for underwater use. Unlike rigid systems that require bulky pressure vessels, some soft electronics have operated directly in high-pressure environments, offering increased functionality.[49,50] LM-based composites are promising in this context, having demonstrated resistance against degradation in aqueous environments,[51] as well as successful implementation in recyclable underwater LM circuits[52] and underwater sensing devices.[45] Taken together, these studies highlight the potential of LM soft circuits as robust, multilayered components for next-generation wearables, combining stretchability, environmental resilience, and advanced sensing.

Here, we advance textile-based wearable electronics by developing elastomer-encapsulated, multilayer circuits that integrate both liquid metal interconnects and rigid components into textile substrates, and we systematically characterize their electromechanical performance, interlayer adhesion, and environmental durability. The integration of circuit components with textiles through soft, extensible circuits allows many electronic and sensing components to interconnect while remaining conformable to serve as wearable electronics. This allows them to leverage advanced functionalities through traditional surface-mounted components and integrated circuits, and their multilayer construction with interlayer vias allows greater flexibility in circuit design. Strong interlayer adhesion, both between the elastomer circuit layers and to the textile substrate, provides wearable electronics with a robust encapsulation and protection against challenging environments. This encapsulation allows the textile-integrated LM soft circuit to intrinsically be used underwater, even while retaining its ability to stretch and flex alongside complex electrical operation. With this, we can create wearable electronics with both stretchable wiring and rigid electronic components that are integrated with form-fitting clothing and conformable to the human body, offering a method to achieve highly interconnected networks with advanced sensing capabilities (Fig. 1(a)).

Results and discussion

Fabrication of multilayer textile-integrated LM soft circuits

For the construction of wearable electronics through elastomer-integrated textiles, a matrix material is required to both serve as a medium between LM wires and textiles and as protection against the external environment. Styrene-based block copolymers, such as styrene–isoprene–styrene (SIS), styrene-isobutylene-styrene (SIBS), and styrene–ethylene/butylene-styrene (SEBS), are materials of interest for the construction of soft, extensible, and wearable circuits because of their unique elastomeric yet thermoplastic nature. In LM soft circuits, SIS has been used as both a substrate material for LM wires[34,35,53,54] and as a matrix for conductive composites incorporating LMs.[11–13,18,30] SIS block copolymers include segments of polystyrene and polyisoprene that form physical crosslinks which provide the material's cohesion and high elasticity, and they have found commercial use as hot melt pressure sensitive adhesives, a capability which we leverage here.[55–58] Because the interactions between polymer chains in SIS can be disrupted by either heat or solvent, the material can be processed in a variety of ways including molding, thermal welding, and coating processes.[21,47,59,60] Here, we use SIS as a substrate material for circuit construction as it allows for heat press processing to textiles, self-adhesion through solvent welding for the addition of further layers, and protection against damage.

The steps of the textile-integrated LM soft circuit fabrication scheme are shown through the construction of a representative six-layer circuit (Fig. 1(b) and Fig. S1, ESI†). To begin, a sheet of SIS elastomer is bonded to a textile substrate through heat press processing. This technique achieves strong adhesion and provides a foundation upon which the circuit is constructed. LM, in this case eutectic gallium–indium (EGaIn), is deposited through spray-coating with a stencil mask. To add additional layers, sheets of SIS are laser cut to include *via* holes and spaces for rigid components. These sheets are aligned and bonded to the circuit by solvent welding with toluene. LM for subsequent circuit layers is deposited and further SIS sheets are stacked until all layers have been completed; this process could include as many layers as are needed. Rigid electronic components are placed in the prepared spaces after all layers are deposited, and the completed circuit is encapsulated by casting further SIS over the prior layers and rigid components. A sample circuit with same design as the schematic is fabricated, in which six light emitting diodes (LEDs) are placed, each on one of six layers, with vias in between (Fig. 1(c)). This forms a series

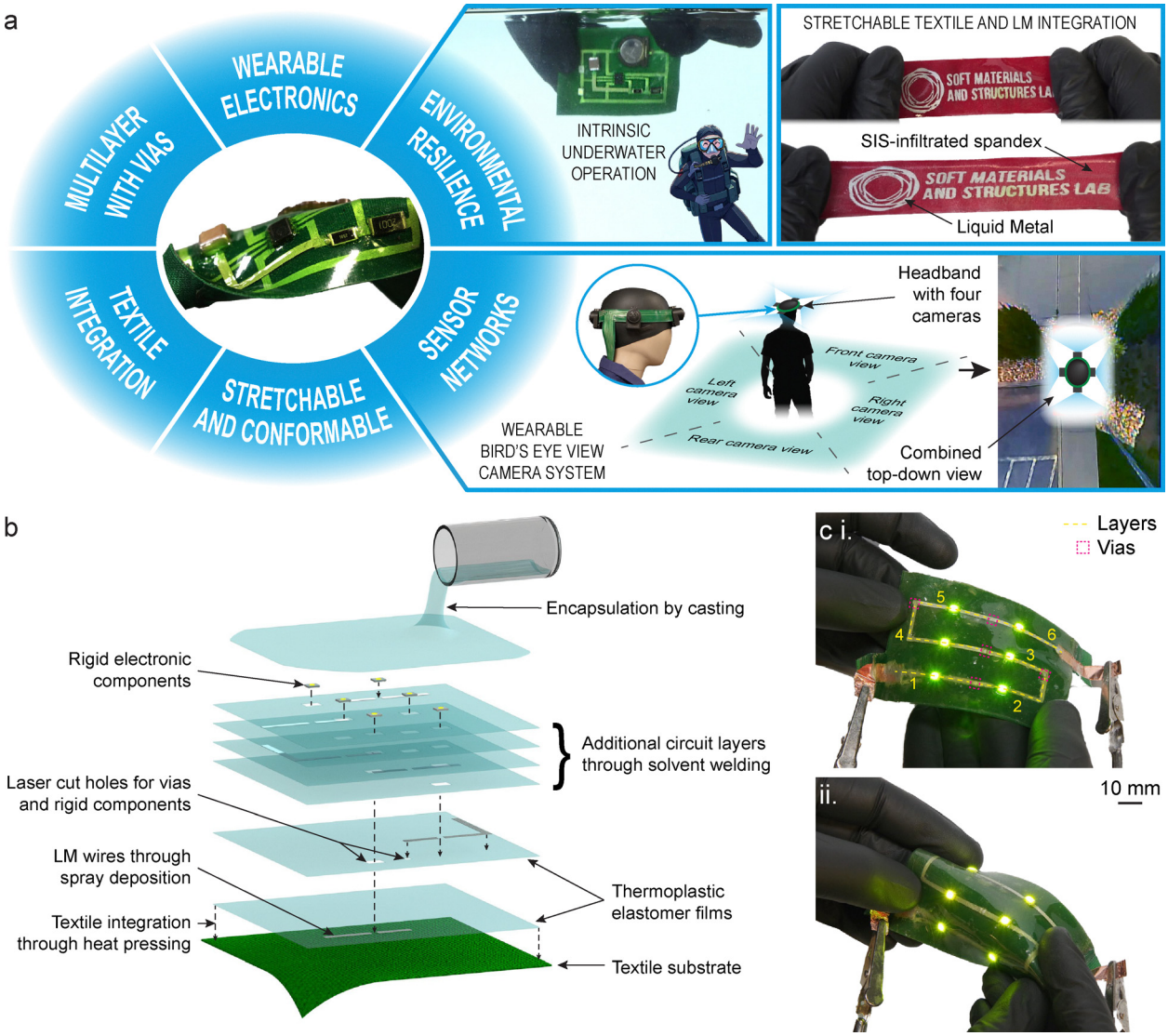

Fig. 1 Overview of textile-integrated LM soft circuits. (a) Capabilities enabled for wearable electronics, including intrinsic underwater operation (top center), stretchability (top right), and a wearable bird's eye view camera system (second row). (b) Layup of a multilayer textile-integrated LM soft circuit with rigid components embedded. (c) Images of a circuit with six LEDs in series, where each is on a different layer with a *via* between, in its (i) normal state and (ii) folded.

circuit of LEDs in which all successfully turn on when external power is applied. This fabrication scheme also allows for circuits to be stretchable when constructed using an extensible textile such as spandex (Fig. 1(a) upper right and Video S1, ESI†). Our approach, which enables textile integration with strong adhesion, multilayer soft circuits with vias that are extensible and conformable, and rigid electronic component implementation, provides a robust scheme for wearable electronics.

Adhesion of elastomer layers and textiles

Robust adhesion between elastomer films and textile substrates can be obtained by heat press processing of SIS films to a variety of textiles (Fig. 2(a)). Adhesive fracture energies are found through T-peel testing to be consistently greater than 1000 J m^{-2}, and even exceeding 11 000 J m^{-2} for a 1000 denier polyester. These are calculated from the steady-state plateau region of the force-extension curve measured during peeling (Fig. 2(a) inset) using the function $G_c = 2F_c/w$, where G_c is adhesive fracture energy, F_c is the steady-state force, and w is the width of the T-peel specimen, with adjustments for extensibility of textile adherends forgone.[61] Optical microscopy demonstrates that elastomer infiltrates better into noncoated textiles of both woven and knit varieties, leading to generally higher adhesion values (Fig. 2(b) and Fig. S2, ESI†). In coated textiles such as polyester (Fig. 2(b)-i and ii), the elastomer remains at the surfaces. This leads to an increased dependence on the surface topography and compatibility, whereas textiles without coatings or a less dense weave, such as polyester spandex (Fig. 2(b)-iii) or cotton (Fig. 2(b)-iv), achieve high

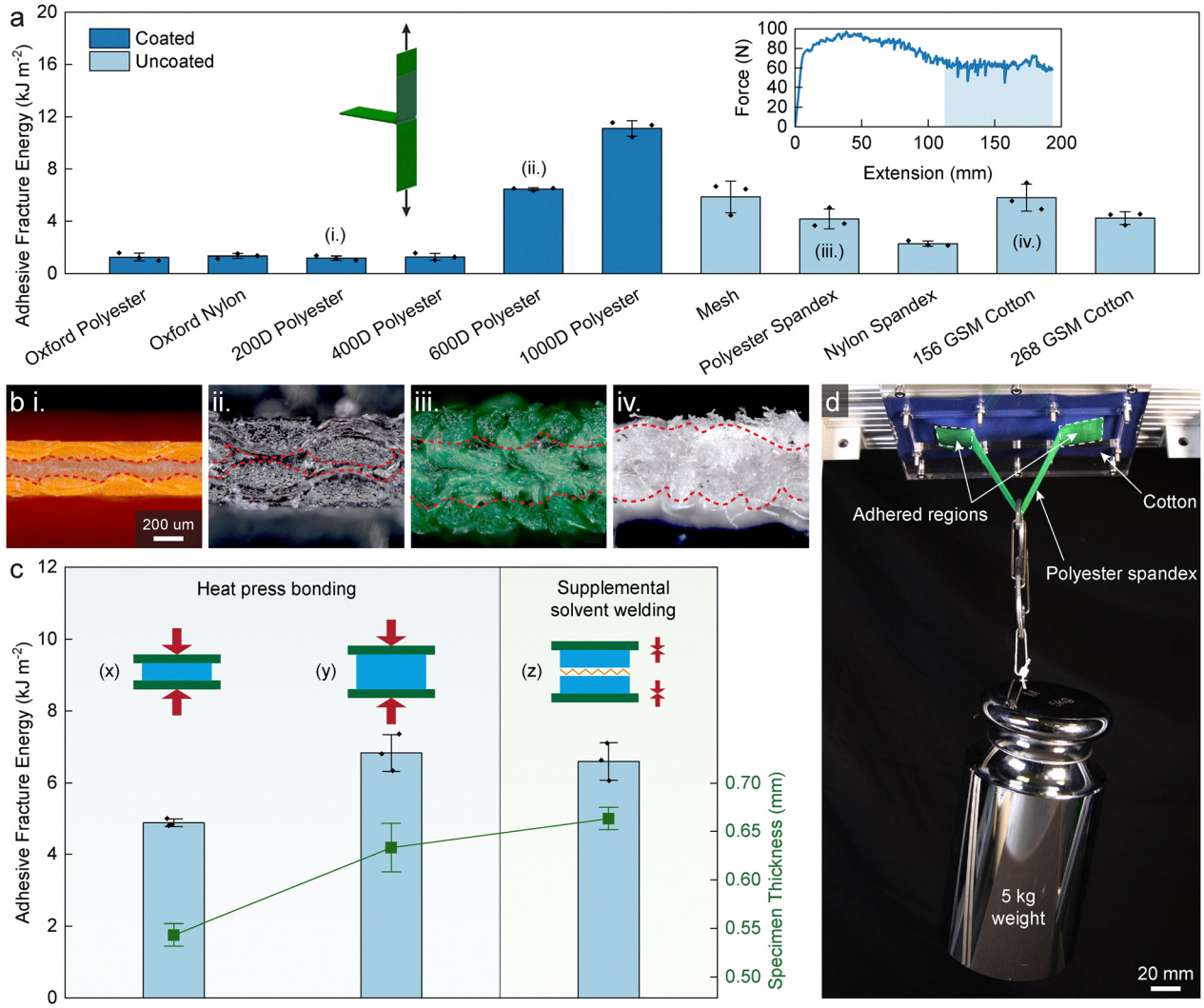

Fig. 2 Adhesion of elastomeric substrate to textiles. (a) Adhesive fracture energy for adhesion of SIS to various textile adherends. Error bars represent 1 s.d. for n = 3 measurements. Insets display a schematic of a T-peel specimen and an example force-extension curve on 156 GSM cotton. Adhesive fracture energy is calculated from the steady-state plateau region of the curve (highlighted). Labels i–iv correspond to the (b) micrographs of the side view of T-peel samples of (i.) 200 denier polyester, (ii.) 600 denier polyester, (iii.) polyester spandex, and (iv.) 156 GSM cotton. Red dashed lines indicate the greatest extent of elastomer impregnation. (c) Adhesive fracture energy of (x) a single layer of SIS heat pressed to textile adherends, (y) two layers of SIS heat pressed to textile adherends, and (z) two textile-integrated layers of SIS with a solvent welded interface between. Error bars represent 1 s.d. for n = 3 measurements. (d) A 5 kg weight hangs from an adhesive joint on an elastic textile.

adhesive strengths due to a greater ability to infiltrate and interlock within the threads. Further information on the textile weaves, materials, coatings, and thread weights can be found in Table S1 (ESI†).

While heat press processing provides strong bonding to a textile substrate, its high process temperature and compressive stress are not conducive to the construction of additional soft circuit layers which include LM wires and rigid components. Instead, solvent welding provides a powerful technique to adhere further layers of SIS to the SIS-textile substrate. Fracture energy is therefore quantified for a textile-integrated structure that also includes solvent welding. Here, heat press bonded T-peel samples of two thicknesses, made using either one or two layers of SIS (Fig. 2(c)-(x) and (y), respectively) are compared to a T-peel sample which includes a solvent welded interface between two layers of textile-bonded SIS (Fig. 2(c)-(z)). The sample which includes a solvent welded interface was constructed by first heat press processing SIS to a single textile adherend, thus leaving an open surface of elastomer, then taking two of those and welding them together with toluene to form a T-peel sample. A comparative analysis of these reveals that the interlayer adhesion achieved through solvent welding between layers of SIS exhibits at least comparable strength to that of integration with textile substrates by heat press processing. Since an increase in thickness of the adhesive provides a greater volume with which to dissipate energy during fracture, the data point for solely heat press processing using two layers of SIS is provided in which the thickness is similar to the solvent welding sample; thickness values of test specimens were measured to confirm parity (Fig. 2(c) right y-axis).

Additionally, the crack propagation during T-peel testing occurred along the elastomer-textile interface even in the test specimens with the added solvent welded interface.

To further demonstrate the high strength of our adhesion to textile substrates, a 5 kg mass is hung from a structure using this adhesion process (Fig. 2(d)). Here, a rigid textile is mechanically fixed to a superstructure, and an adhered strip of spandex supports the hanging weight with only two adhered regions of 25 × 25 mm each. This high strength of adhesion enables robust textile integration of our wearable circuits to prepare them for rugged applications such as underwater use. Both the heat press processing and solvent welding techniques prevent delamination of the LM soft multilayer circuits, ensuring they both remain affixed to the textile substrate of interest and maintain their cohesion between layers.

Stiffness of multilayer textile-integrated system

This adhesion allows textiles to be integrated with SIS-based LM soft multilayer circuits which can stretch and fold while remaining operable. The extensible substrate textiles (spandex, mesh, and cotton jersey materials) serve not only to provide integration into garments, but also serve as a mechanical reinforcement for stretchable soft circuits. Knit textiles offer extensibility beyond that of their constituent fibers through a looped structure, in which gaps between fibers open.[62] However, the exact mechanical properties of a textile-elastomer structure are influenced by complex geometry, material interfaces, and nonlinear effects[63]. Thus, how these nonlinear textile mechanics influence the ultimate compliance of our textile-integrated LM soft circuits needs to be investigated.

We observe that the mechanics of the textile-elastomer system under uniaxial strain vary greatly depending on the direction of loading relative to the knit pattern (Fig. 3(a)). The effect of integrating elastomer is different in each knit textile direction. When loaded in the wale direction (in the lengthwise direction, and parallel to the selvage edge), the stiffness is significantly increased at lower strains (Fig. 3(b)-i) but the structure is weakened, both in a reduction of ultimate tensile

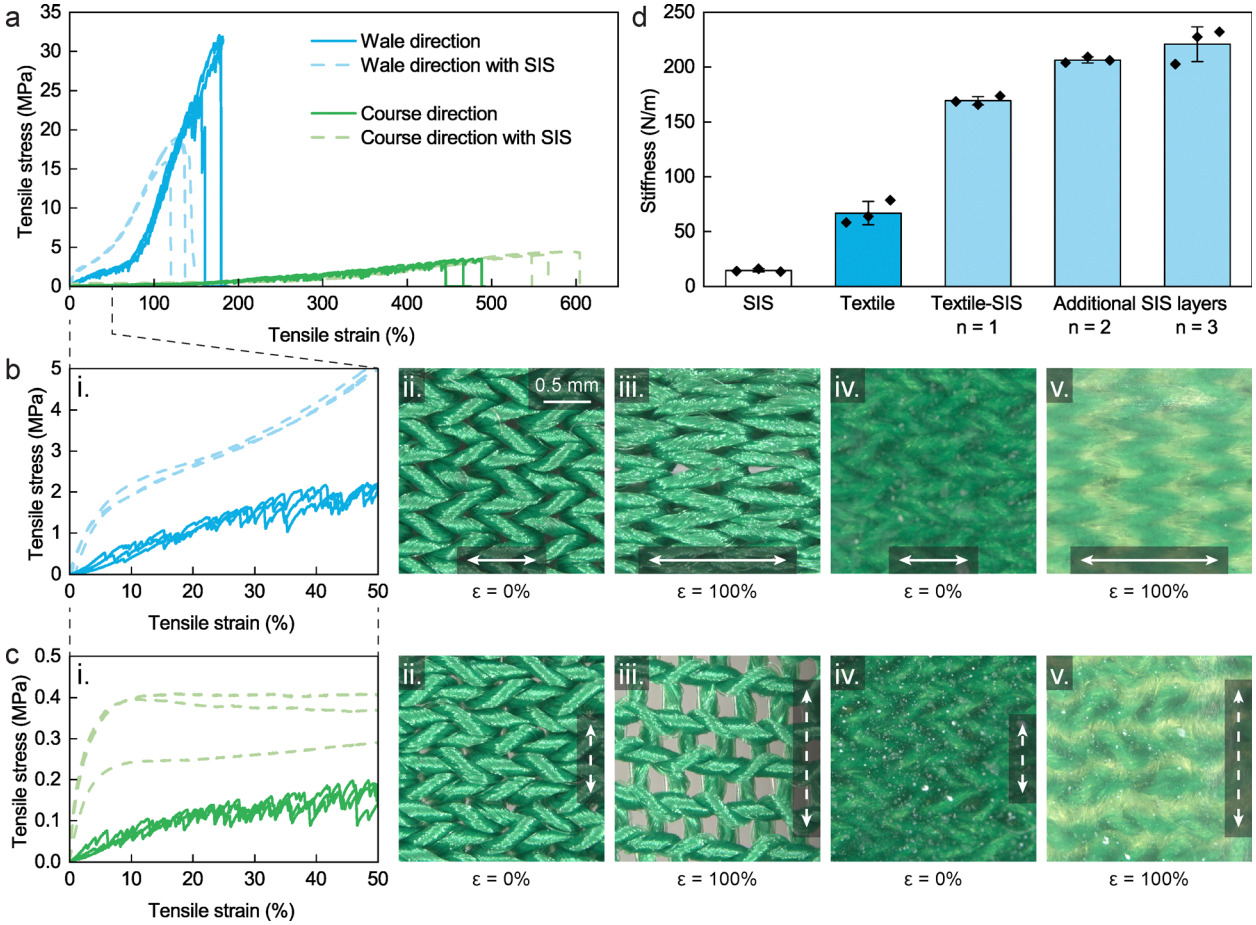

Fig. 3 Mechanical characterization of textile-elastomer substrate. (a) Stress–strain curves for polyester spandex textiles under uniaxial tension in the wale and course directions, both with and without SIS adhered. (b) (i) Stress–strain curves up to 50% strain for loading in the wale direction. Microscope images of wale-strained textile at (ii) ε = 0% and (iii) 100% and textile-elastomer substrate at (iv) ε = 0% and (v) 100%. (c) (i) Stress–strain curves up to 50% strain for loading in the course direction. Microscope images of course-strained textile at (ii) ε = 0% and (iii) 100% and textile-elastomer substrate at (iv) ε = 0% and (v) 100%. (d) Stiffness (taken at 50% strain) for SIS, polyester spandex textiles strained in the wale direction as is and with added layers of SIS. Error bars represent 1 s.d. for n = 3 measurements.

strength and strain at break. When loaded in the course direction, (in the crosswise direction) the material is much more compliant than in the wale direction and the stress–strain response is similar to that of the textile alone. The elastomer still provides an increase in stiffness at low strains (Fig. 3(c)-i), but this becomes negligible at higher strains. In contrast to loading in the wale direction, the elastomer acts to strengthen the material when loading in the course direction, as it is capable of withstanding greater stresses and strains when elastomer is integrated. These varying changes to the mechanical performance of a textile-elastomer system compared to either of its constituents suggests that in knit textiles, the manner in which elastomer infiltrates the textile structure results in a composite-like response rather than a layered response (Fig. 3(b) and (c)-ii–v).[63,64] This further varies significantly across different extensible textile materials integrated with elastomer (Fig. S3, ESI†). Because many of the textile structures exhibit non-homogeneous strain distributions by opening up gaps between threads when stretched[62] (Fig. S4, ESI†), the mechanics could be altered through the infiltration of elastomer between the textile fibers.

With this fabrication method for multilayer textile-integrated LM soft circuits, each added layer expands the circuit's functional complexity through additional routing, sensing, or interfacing capabilities, while only reducing deformability of the device to a lesser extent through slight increases in overall thickness. To understand how additional layers impact compliance, we measure the stiffness at 50% strain in the wale direction, representative of upper-bound deformations in typical wearable use cases, for devices with varying numbers of elastomer circuit layers (Fig. 3(d)). While the first elastomer layer introduces the greatest increase in stiffness through embedding into the textile, subsequent layers contribute more modestly, indicating that the added layers behave mechanically as discrete additions rather than forming a fully bonded composite structure. This layered architecture preserves overall compliance while enabling increased functional density. This structure–mechanics–functionality relationship allows for the integration of complex soft circuits with multilayer interconnects and hybrid components with dramatic deformability, enabling greater functionality without compromising ergonomics.

Electromechanical properties of textile-integrated LM soft circuits

To evaluate the applicability of textile-integrated LM soft circuits in highly stretchable textiles such as spandex, electromechanical characterization was performed. In these tests, a single representative wire of the LM soft circuit, encapsulated between elastomer layers formed into tensile dogbones, is extended under tensile loading while the resistance is measured with a four-point probe. Samples for these tests include both elastomer and LM only, and ones integrated with a textile layer (polyester spandex). The LM-elastomer system (SIS-LM wire) is shown to stretch to greater than 2000% strain at fracture under tensile loading, while the addition of a bonded stretchable textile layer (SIS-LM wire on spandex) reduces this to about 600% strain (Fig. 4(a)-i and Fig. S5, ESI†).

Normalized resistance (R/R_0), the electrical resistance (R) relative to the initial undeformed state (R_0), is measured over the same tensile extension (Fig. 4(a)-ii). Here, the specimens bonded to textile substrates show electrical failure of the LM wire at lower strains than material fracture. For all cases, system conductivity is lost prior to specimen fracture due to discontinuities developing in the LM wire that prevent a continuous conductive pathway. One textile-bonded test specimen retains some conductivity up until mechanical failure at about 600% strain, but prior to that showed a sharp increase in electrical resistance above 250% strain. Both samples with and without textile layers show similar electromechanical trends at low strain ($\sim$100%), indicating that the integration of a textile layer for LM soft circuits does not degrade conductivity at the strains expected in wearable electronics. This suggests that the relationship between the layup of the structure and the electromechanics of a LM wire does not have an influence at low strains. At higher strains, the specimens with bonded spandex begin to lose conductivity prior to specimens of just elastomer and LM. This may be due to highly localized stress concentrations resulting from the nonlinear deformation response of stretchable knit textiles and their interaction with the elastomer integrated between their fibers. Even with the addition of rigid components such as LEDs, the textile-integrated LM soft circuit retains functionality at strains of up to 300% (Fig. 4(b) and Video S1, ESI†).

To further investigate the mechanics driving electrical continuity disruption, we examine LM wires subject to uniaxial strain under a microscope. For LM wires without encapsulation, we observe the emergence of gaps normal to the direction of the applied tension (Fig. 4(c)). These gaps provide an explanation for why resistance sharply increases at different strains for each specimen in the electromechanical data previously measured (Fig. 4(a)-ii); since a disruption of electrical continuity could be caused by propagation of only a single gap across the entire width of the LM wire, the presence of many gaps in even only 1 mm of LM wire leads to this failure being highly driven by probability. When encapsulated by elastomer, it appears that these gaps may not form as readily (Fig. 4(d)). Additionally, the stretchable knit textiles exhibit significant out-of-plane bending (*i.e.*, curling) at high strains, which may also contribute to the electromechanical performance.

Textile-integrated specimens are also subjected to a cyclic folding test (Fig. 4(e) and Video S2, ESI†) and a cyclic tensile test (Fig. S6, ESI†), and show stable behavior. This measures the resilience of soft circuits subjected to the manipulation they would see in use, as this response can be dependent on the materials present.[65–71] For textile-integrated LM soft circuits, resistance is shown to have minimal change over 1000 cycles of folding (Fig. 4(e)-i). Both stretchable and inextensible textiles were investigated across 5 test specimens each (Fig. S7, ESI†), with a single, median representative being presented. The darker line is a running average representing the overall trend in resistance, while the shaded region represents the resistance change during each fold (see also Fig. 4(e)-ii). The inextensible textile backings exhibited a slightly greater tendency to cause

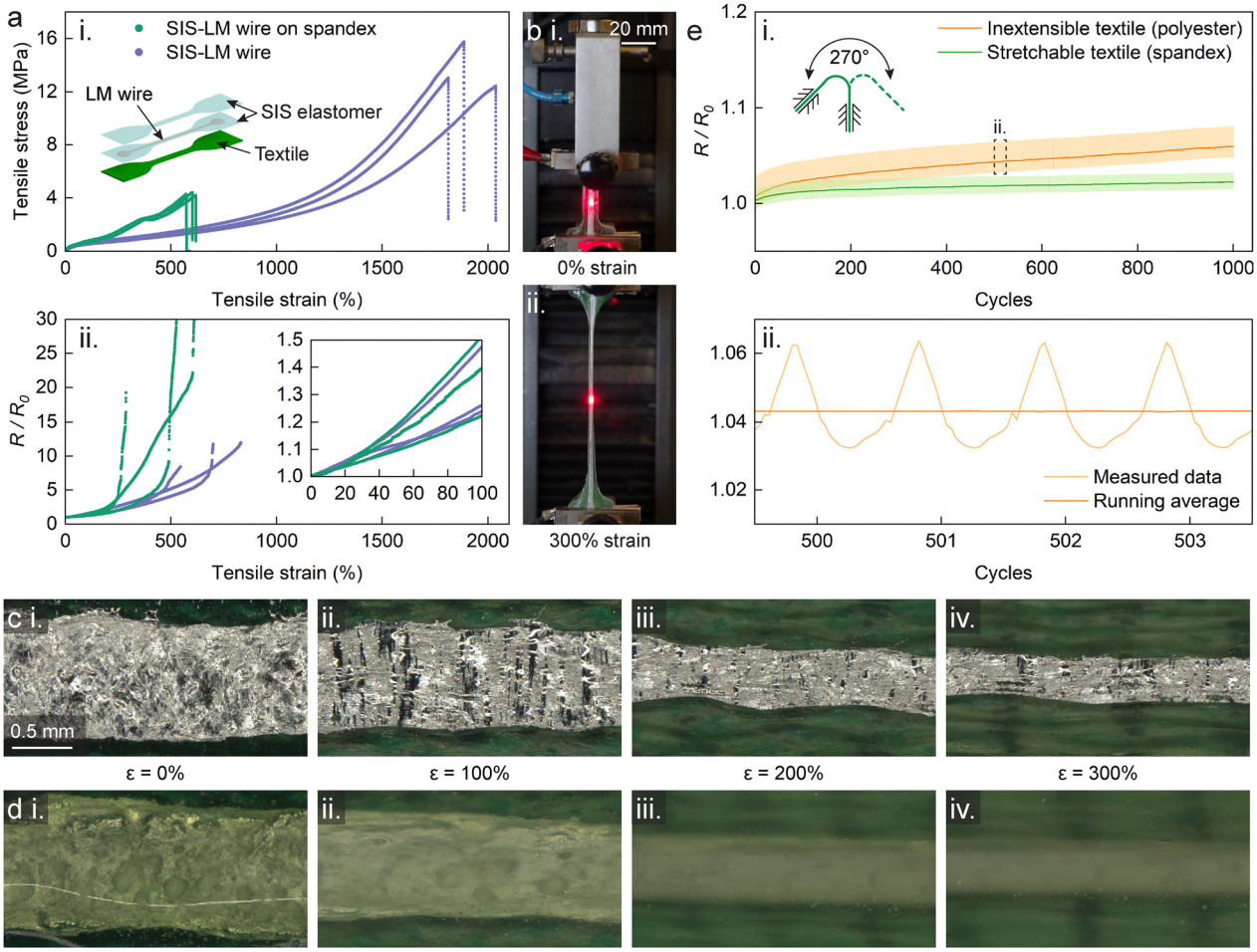

Fig. 4 Electromechanical characterization of textile-integrated LM soft circuits. (a) (i) Tensile mechanical response of LM wires in the soft circuits, both with and without bonded textile. Inset depicts sample layout. (ii) Normalized resistance for same specimens as in (i). Inset shows initial range from 0 to 100% strain during which minimal change occurs. (b) Demonstration of a textile-integrated LM soft circuit with a rigid LED structure on a polyester spandex substrate strained to 300% of original length. (c) Microscope images of a LM wire on elastomer-integrated textile at (i) ε = 0%, (ii.) ε = 100%, (iii) ε = 200%, and (iv) ε = 300%. (d) Microscope images of a LM wire on elastomer-integrated textile and encapsulated by further elastomer at (i) ε= 0%, (ii) ε = 100%, (iii) ε = 200%, and (iv) ε = 300%. (e) (i) Normalized resistance during 1000 cycles of folding, with inset displaying test setup, and (ii) measured data and running average for 3 representative cycles.

an increase in resistance over time. This further shows that the integration of elastomer and textile enables LM wires to retain their electrical properties and functionality during use. This enables a textile-integrated LM soft circuit system that is robust against manipulation such as stretching and folding, which provides desirable properties for use in wearable electronics.

Application of textile-bonded LM soft circuits to underwater environments

By fully encapsulating the soft circuit, these textile-integrated wearable electronics are resistant to aqueous environments. We demonstrate this by immersing circuits in water, during which the circuits retain functionality. This includes a tensile test after water immersion for 24 hours, showing no change in the electromechanical nor mechanical response of the LM wire (Fig. S8, ESI†), as well as a test of ingress protection against water based on the IPX7 rating in the IEC 60529 standard (Fig. 5(a) and Video S3, ESI†), which demands submersion to a depth of 1 meter for 30 minutes to evaluate water resistance. We immerse a fully encapsulated textile-integrated LM soft circuit consisting of a battery, resistor, and LED to this depth and record it with a camera and timer. Continual operation of the LED is shown during the entire duration, demonstrating successful protection against water damage under the same conditions as a standardized rating for consumer electronic devices. Furthermore, we show stable functionality of textile-integrated and encapsulated LM wires immersed in hot and cold environments, including 0 °C freezing water, 50 °C hot water, and 80 °C air, with only minimal temperature dependence in the resistivity of the LM wire and a return to its original properties after temperature exposures (Fig. S9, ESI†).

The integration of more complex circuits is shown through the construction of an alternating flash LED circuit utilizing an IC, onboard power, and multiple rigid electronic components (Fig. 5(b)). This circuit includes an 8-pin timer IC, a coin cell

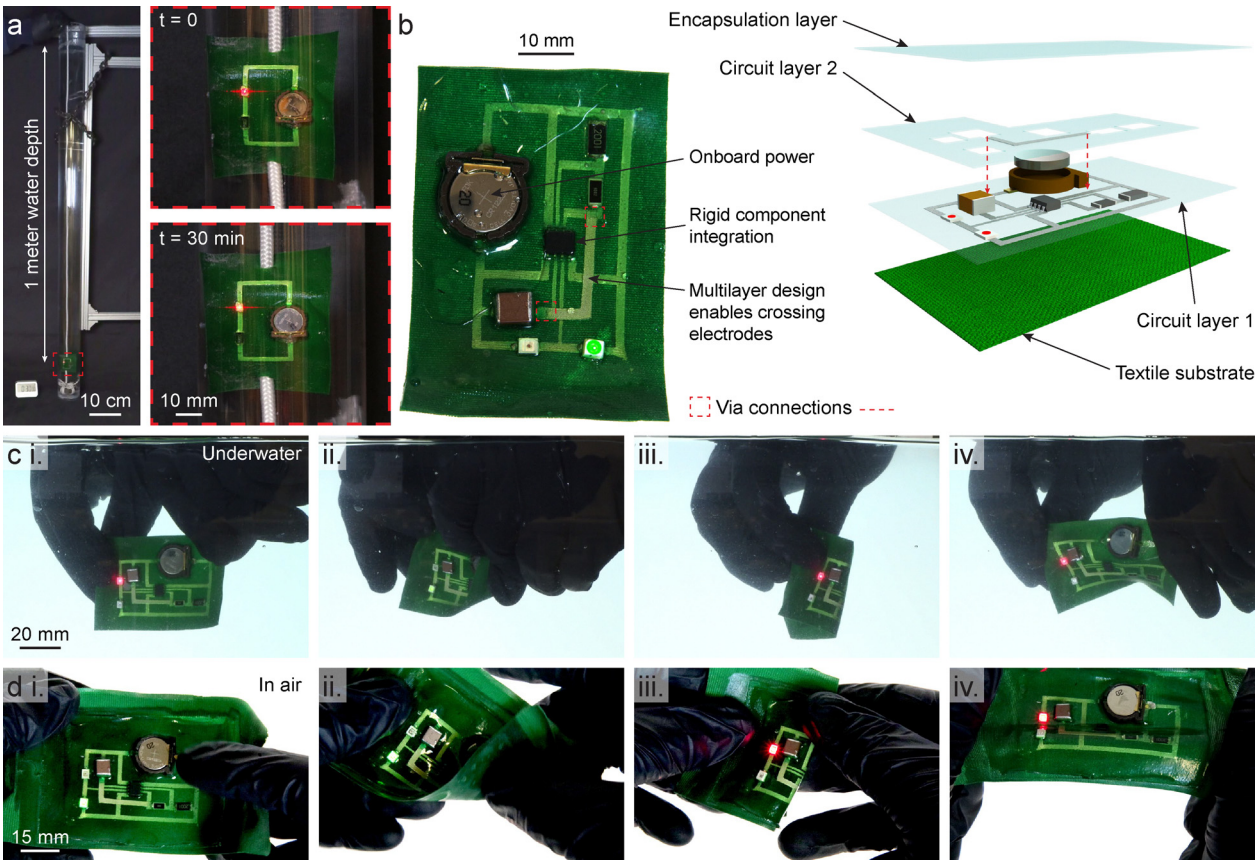

Fig. 5 Underwater demonstrations of flexible and stretchable textile-integrated LM soft circuits. (a) IPX7 water immersion test of a representative circuit, which is still functioning after 30 minutes at a depth of 1 meter. (b) Sample two-layer circuit in which two LEDs blink in alternate using a 555 timer chip, and (c) its operation in underwater and (d) dry environments, including (ii), (iii) folding and (iv) stretching.

battery, and resistors and capacitors which make a pair of red and green LEDs flash in an alternating pattern. Due to the required connections, this circuit would not be possible in a single-layer configuration using this specific model of timer IC, and multiple vias are used to allow LM soft conductive traces to cross over each other in a multilayer design. The elastomer encapsulation enables this circuit to operate when immersed in water, including still being foldable and stretchable (Fig. 5(c), (d) and Video S4, ESI†). This inherent water resistance is enabled by the elastomer encapsulation, which neither absorbs water (Fig. S10, ESI†) nor permits the transmission of water vapor (Fig. S11, ESI†). The capability of these textile-integrated LM soft circuits to survive submersion in water without additional protective structures or potting compounds shows potential for their use in more varied applications, such as wearable components on dive suits or as part of soft underwater robots. Furthermore, by removing rigid–rigid interfaces, soft circuit structures such as these show future possibilities for hydrostatic pressure resilient electronic systems.[72] Thus, in addition to multilayer construction and textile integration, this fabrication method also provides multiple benefits through inherent fortification against aqueous environments and hydrostatic pressure for next-generation underwater electronics.

Application of textile-bonded LM soft circuits to wearable sensing

In addition to underwater applications, we also demonstrate the ability of these textile-integrated LM soft circuits to facilitate advanced wearable electronics capable of functions such as environmental sensing. Using a multilayer LM soft circuit bonded to an extensible textile, we create a wearable device that provides a user with a complete overhead bird's eye view of their surroundings in all directions. This device is designed as a conformable and unobtrusive headband-like garment which serves as a mounting point for four orthogonally-facing cameras (Fig. 6(a)). Each camera requires a devoted power, ground, and analog signal wire connected to a processor, which warps and stitches the video feeds into the overhead view; this is provided through a circuit containing two layers with six traces of LM wiring each for a total of 12 traces, with a sum total of 4.2 meters of LM wiring throughout (Fig. 6(b)). The LM wiring is capable of transmitting 25 frames per second (through a phase alternating line protocol) from four cameras to the central processor, demonstrating the capability of the LM wires to carry large amounts of data in real time over extended lengths.

The camera system is trialed in outdoor (Fig. 6(c) and (d)) and indoor (Fig. 6(e) and (f)) environments. In both open and

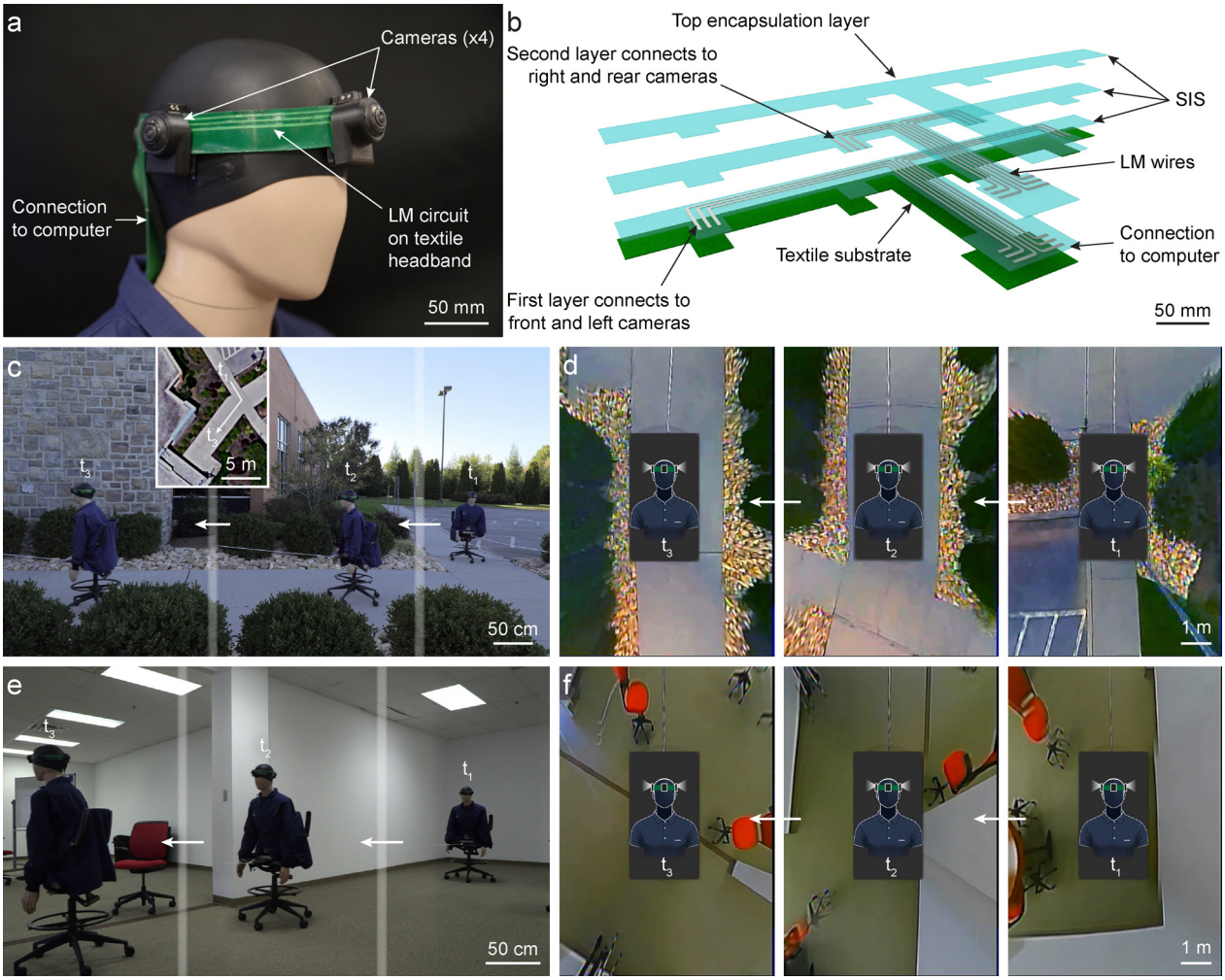

Fig. 6 Applications of textile-integrated LM soft circuits to wearable sensing. (a) Image of headband with four cameras placed on a mannequin. (b) Exploded-view schematic of wearable headband circuit. (c) Demonstration of the four-camera headband system being moved through an outdoor environment while (d) recording a stitched overhead view, shown at three different times, t_1, t_2, and t_3. Inset image in (c) shows satellite view of area (Maps data: Google 2024). (e) Demonstration of the four-camera headband system being moved through an indoor office space environment while (f) recording a stitched overhead view, shown at three different times, t_4, t_5, and t_6.

constrained environments, the wearable bird's eye view system is capable of collecting and recording not only the four independent camera views, but also the stitched overhead view (Video S5, ESI†). Additionally, the stitched overhead view is provided in real-time to an external screen. This wearable device expands beyond current body camera technology in that it provides information in real time for situational awareness and can record 360° context for body cameras used for incident recording. The networking of multiple body cameras together using LM wires to transmit power and data enables new functions like the overhead bird's eye view in wearable sensing, but also shows potential for multiple wearable sensors to form sensor networks, such as for health monitoring or situational awareness. This type of sensor fusion can greatly benefit from the ability to create advanced, multilayer circuits that are integrated with textiles, and this textile-integrated process provides a foundation for the addition of advanced sensor networks to garments.

Conclusions

We create LM soft circuits which achieve robust adhesion to textiles, are foldable and stretchable, can use multilayer designs with vias as well as many rigid components, and survive submersion in water. We characterize critical mechanisms in textile-integrated soft circuits, including how textiles impact electromechanical performance of stretchable conductors, which informs how these techniques can be employed for wearable electronics across a range of applications. The use of multiple adhesion techniques enables our circuit construction, as both heat press processing and solvent welding are employed together to achieve strong interlayer adhesion within textile-integrated LM soft circuits. Using both techniques grants the ability to create multilayer circuits in our scheme without limiting the adhesion either to textiles or between circuit layers, ensuring the entire multilayer circuit has a robust construction. The structure–mechanics–functionality relationship we characterize for this layup allows

for multilayer circuit designs to enable increases in functionality without significant penalties to deformability. For manipulations expected of wearable electronics, these textile-integrated circuits are shown to maintain electrical continuity under both extension and folding, as LM can deform and flow along with multiaxial mechanical strains. This provides a reliable interconnect between circuit elements for wearable electronics, including resistances low enough to enable longer transmission distances. Environmental resilience is also shown through submersion in water, demonstrating the inherent ruggedness of these soft circuits and their benefits for underwater wearables.

With this method, wearable electronics can be made to suit many different complex applications, such as our wearable bird's eye view imaging system. Multilayer construction enables the manufacture of complex soft circuits, as does the integration of many types of rigid components; many electronic functionalities are not possible with the single-layer-only designs present in many prior works on LM soft circuits. As improving circuit complexity is currently a primary challenge in the LM field, advancement into multilayer LM circuits and manufacturing methods is crucial. Additionally, the fabrication method uses techniques such as lamination and spray deposition that could be integrated into high-speed, roll-to-roll manufacturing processes in future work. By using the adhesion of multiple elastomer layers and the extensibility and conformability of LM wires to create stretchable soft circuits which are robustly integrated with textiles, a new scheme for wearable electronics is achieved with both ruggedness for various environments and multilayer construction for advanced wearable devices.

Experimental

LM fabrication

Eutectic gallium–indium (EGaIn) liquid metal was made by combining a 3 : 1 by mass ratio of gallium and indium on a hot plate at 200 °C overnight.

SIS sheet fabrication

A 1 : 5 by mass mixture of 35 g SIS pellets (Sigma-Aldrich part 432393) and 175 g toluene was combined in a 250 mL airtight jar and kept on a hot plate at 55 °C with a stir bar until fully dissolved. SIS sheets were made by casting 10 g of SIS:toluene mixture into a 110 mm by 85 mm laser cut acrylic (McMaster part 8589K42) mold coated in mold release (Ease Release 200). These were left for 24 hours in a fume hood such that the toluene evaporates, and the SIS sheets which remain were removed and demolded by hand. Edges were trimmed to remove any meniscus that formed at the edge of the mold. The thickness of the final SIS sheet is 0.20–0.25 mm.

Heat press processing for SIS and textile adhesion

SIS sheets used in adhesion tests were adhered to textiles using a heated press (Carver Bench Top Model 4120) at 200 °C and 500 kPa for 3 minutes. To achieve a smoother surface for use in demonstration samples utilizing LM, some samples were prepared at only 150 °C. The processing parameters for hot melt adhesion were determined through an investigation using Box–Behnken methods on several textiles; results were generalized to the full selection of textiles using a scoring system (Fig. S12, ESI†).

Textile-integrated LM soft circuit fabrication

SIS sheets for each layer were cut to desired size with holes for vias and rigid components using a laser cutter (Universal Laser Systems VLS4.75). Spray masks (Blazer Orange Laser Mask, Johnson Plastics Plus) were cut to the desired trace pattern for each layer. LM was spray-coated with an airbrush onto the first layer (SIS sheet heat pressed to textile) using a mask. Toluene is applied to the surface using a misting spray bottle, and the next SIS layer is placed on top in alignment with the circuit pattern. Toluene is evaporated by leaving the circuit in a fume hood overnight. LM is spray-coated onto the second layer with the proper mask for its desired pattern. This process is repeated for any subsequent layers as desired.

Once all layers are made, rigid components are placed and the circuit is encapsulated by either solvent welding another SIS film or casting additional SIS:toluene mixture on top.

Adhesive peel testing

Adhesion was measured using T-peel geometry based on ASTM D1876 on an Instron 5944 Universal Testing Machine. Samples were prepared in panels 75 mm wide by 175 mm long, bonded over 100 mm of their length. Three test specimens were cut from each panel to a width of 25 mm. Adhesive fracture energy was calculated using $G_c = 2F_c/w$, where F_c is the critical force in the steady-state plateau region of the load–displacement curve during peel (see inset of Fig. 2(a)).

Tensile electromechanical testing

Sheets of SIS and SIS bonded to polyester spandex (Fabric Wholesale Direct SKU SV578475) were cut into tensile dog bone specimens of 50% size of the ASTM D412 type C standard using a die cutter. Copper tape was applied the ends of a specimen, and LM was deposited as a single soft wire using a spray mask and airbrush. Another SIS dog bone specimen was applied *via* solvent welding with toluene to encapsulate the LM soft wire. Specimens were tested using a Instron 5944 Universal Testing Machine at a rate of 60 mm min^{-1} until mechanical fracture, and the electrical resistance was simultaneously measured by a Keithley 2461 SourceMeter connected to the copper tape interfaces at each end of the LM soft wire.

Cyclic folding electromechanical testing

Sheets of SIS and SIS bonded to polyester spandex (Fabric Wholesale Direct SC578446) and 600D Polyester (Rockywoods RBC600) were cut into rectangles of 10 × 100 mm using a laser cutter. Copper tape was applied the ends of a specimen, and LM was deposited as a single soft wire using a spray mask and airbrush. Another layer of SIS was applied *via* solvent welding with toluene to encapsulate the LM soft wire. Specimens were

tested using a custom setup consisting of a position control motor (DYNAMIXEL XC430-T150BB-T) and 3D-printed grips (Bambu Lab P1S and Verbatim #55000 ABS filament), which rotates across a 270 arc (Video S2, ESI†). The electrical resistance was simultaneously measured by a Keithley 2461 SourceMeter connected to the copper tape interfaces at each end of the LM soft wire.

Water immersion test

A sample circuit with a CR1220 coin cell battery (Digikey part numbers SY033-ND and 36-1056-ND), LED, and resistor (Digikey part number A116039CT-ND) was prepared. A 4 ft long by 3 in diameter plastic tube (McMaster part number 9176T17) was sealed at one end and filled with tap water. The circuit was attached to a weighted line and inserted into the water-filled tube such that it was at a depth of 1 m, while being observed by a camera for continuous operation of the LED for 30 minutes.

Wearable sensing headband fabrication

The wearable sensing headband circuit was fabricated in a flat configuration on a polyester spandex substrate using the methods previously described. During fabrication, copper tape was placed at the terminus of each LM soft wire, and a mixture of 5 volume percent copper powder (US Research Nanomaterials stock # US5002) in LM was applied in a small amount at the soft–rigid interface. In addition, the circuit was annealed in a 80 °C oven for approximately 72 hours after assembly to relieve residual stresses. Cameras (Weivision 360 Surround View System, Amazon part number B00ZR65O2G) were affixed to mounting brackets fabricated through 3D printing that clamp onto the headband, and their connection wires were soldered to the copper tape. An additional sheet of SIS was applied through solvent welding to connect the two ends of the circuit, forming the headband shape. The wearable circuit is connected to a mini-computer which computes the stitched overhead view. This system is powered by a battery (Turnigy 12000 mAH 4S LiPo pack, HobbyKing SKU 9067000425-0).

Author contributions

B. T. W. and M. D. B. conceived the idea; B. T. W. and E. T. W. designed systems and components with input from M. D. B; B. T. W. and E. T. W. fabricated components and performed experiments; B. T. W. and E. T. W. and analyzed data; B. T. W., E. T. W. and M. D. B. wrote the paper; and M. D. B. supervised the study.

Conflicts of interest

The authors declare no competing interests.

Data availability

Data available on request from the authors.

Acknowledgements

We acknowledge support from the Office of Naval Research (N000142112699 and N000142412504).

References

1 S. W. Chung and H. T. Kim, Interfacial reliability between hot-melt polyamides resin and textile for wearable electronics application, *Microelectron. Reliab.*, 2012, **52**, 1501–1510.
2 S. de Mulatier, M. Nasreldin, R. Delattre, M. Ramuz and T. Djenizian, Electronic Circuits Integration in Textiles for Data Processing in Wearable Technologies, *Adv. Mater. Technol.*, 2018, **3**, 1700320.
3 M. von Krshiwoblozki, T. Linz, A. Neudeck and C. Kallmayer, Electronics in Textiles – Adhesive Bonding Technology for Reliably Embedding Electronic Modules into Textile Circuits, Wearable/Wireless Body Sensor Networks for Healthcare Applications, 85, 1-10, 2012.
4 E. Heo, K. Y. Choi, J. Kim, J. H. Park and H. Lee, A wearable textile antenna for wireless power transfer by magnetic resonance, *Text. Res. J.*, 2018, **88**, 913–921.
5 H.-J. Kim, R. Lin, S. Achavananthadith and J. S. Ho, Near-field-enabled Clothing for Wearable Wireless Power Transfer, in 2020 IEEE Wireless Power Transfer Conference (WPTC), 22-25, IEEE, nov 2020.
6 T. Araki, M. Nogi, K. Suganuma, M. Kogure and O. Kirihara, Printable and Stretchable Conductive Wirings Comprising Silver Flakes and Elastomers, *IEEE Electron Device Lett.*, 2011, **32**, 1424–1426.
7 B. M. Li, O. Yildiz, A. C. Mills, T. J. Flewwellin, P. D. Bradford and J. S. Jur, Iron-on carbon nanotube (CNT) thin films for biosensing E-Textile applications, *Carbon*, 2020, **168**, 673–683.
8 K. Klamka, R. Dachselt and J. Steimle, Rapid iron-on user interfaces: Hands-on fabrication of interactive textile prototypes, in *Proceedings of the 2020 CHI Conference on Human Factors in Computing Systems*, ACM, 2020, pp. 1–14.
9 T. Vervust, F. Bossuyt, F. Axisa and J. Vanfleteren, Stretchable and Washable Electronics for Embedding in Textiles, *MRS Proc.*, 2010, **1271**, 1271-JJ04-03.
10 E. J. Markvicka, M. D. Bartlett, X. Huang and C. Majidi, An autonomously electrically self-healing liquid metal-elastomer composite for robust soft-matter robotics and electronics, *Nat. Mater.*, 2018, **17**(7), 618–624.
11 R. Tutika, A. B. M. T. Haque and M. D. Bartlett, Self-healing liquid metal composite for reconfigurable and recyclable soft electronics, *Commun. Mater.*, 2021, **2**(1), 64.
12 W. Zu, Y. Ohm, M. R. Carneiro, M. Vinciguerra, M. Tavakoli and C. Majidi, A Comparative Study of Silver Microflakes in Digitally Printable Liquid Metal Embedded Elastomer Inks for Stretchable Electronics, *Adv. Mater. Technol.*, 2022, **7**, 2200534.
13 Y. Li, S. Feng, S. Cao, J. Zhang and D. Kong, Printable Liquid Metal Microparticle Ink for Ultrastretchable Electronics, *ACS Appl. Mater. Interfaces*, 2020, **12**, 50852–50859.

14 L. Ai, W. Lin, L. Ai, Y. Li, M. Qiang, X. Wang, M. Shi, Z. Yang and X. Yao, ''heat-press-n-go'' stretchable interconnects enabled by liquid metal conductor with supramolecular confinement, *Adv. Funct. Mater.*, 2025, **35**(20), 2425264.

15 T. A. Pozarycki, D. Hwang, E. J. Barron, B. T. Wilcox, R. Tutika and M. D. Bartlett, Tough Bonding of Liquid Metal-Elastomer Composites for Multifunctional Adhesives, *Small*, 2022, **18**(41), e2203700.

16 S. Lee, S. A. Jaseem, N. Atar, M. Wang, J. Y. Kim, M. Zare, S. Kim, M. D. Bartlett, J.-W. Jeong and M. D. Dickey, Connecting the dots: Sintering of liquid metal particles for soft and stretchable conductors, *Chem. Rev.*, 2025, **125**(6), 3551–3585.

17 E. B. Secor, A. B. Cook, C. E. Tabor, M. C. Hersam, E. B. Secor, M. C. Hersam, A. B. Cook and C. E. Tabor, Wiring up Liquid Metal: Stable and Robust Electrical Contacts Enabled by Printable Graphene Inks, *Adv. Electron. Mater.*, 2018, **4**, 1700483.

18 A. B. M. Tahidul Haque, R. Tutika, M. Gao, A. Martinez, J. Mills, J. Arul Clement, J. Gao, M. Tabrizi, M. Ravi Shankar, Q. Pei and M. D. Bartlett, Conductive liquid metal elastomer thin films with multifunctional electro-mechanical properties, *Multifunct. Mater.*, 2020, **3**, 044001.

19 A. B. Haque, D. H. Ho, D. Hwang, R. Tutika, C. Lee and M. D. Bartlett, Electrically Conductive Liquid Metal Composite Adhesives for Reversible Bonding of Soft Electronics, *Adv. Funct. Mater.*, 2023, **34**(31), 2304101.

20 T. A. Pozarycki, W. Zu, B. T. Wilcox and M. D. Bartlett, A Flexible and Electrically Conductive Liquid Metal Adhesive for Hybrid Electronic Integration, *Adv. Funct. Mater.*, 2024, **34**(31), 2313567.

21 S. Choi, J. Park, W. Hyun, J. Kim, J. Kim, Y. B. Lee, C. Song, H. J. Hwang, J. H. Kim, T. Hyeon and D. H. Kim, Stretchable Heater Using Ligand-Exchanged Silver Nanowire Nanocomposite for Wearable Articular Thermotherapy, *ACS Nano*, 2015, **9**, 6626–6633.

22 H. Weerathunga, T. T. Do, H. D. Pham, R. Jones, J. Macleod, T. Kim and D. Dubal, Washable and Flexible All Carbon Electrothermal Joule Heater for Electric Vehicles, *Adv. Mater. Technol.*, 2023, **8**(7), 2201538.

23 Y. Song, J. Min, Y. Yu, H. Wang, Y. Yang, H. Zhang and W. Gao, Wireless battery-free wearable sweat sensor powered by human motion, *Sci. Adv.*, 2020, **6**, 9842.

24 H. Chander, R. F. Burch, P. Talegaonkar, D. Saucier, T. Luczak, J. E. Ball, A. Turner, S. N. Kodithuwakku Arachchige, W. Carroll, B. K. Smith, A. Knight and R. K. Prabhu, Wearable stretch sensors for human movement monitoring and fall detection in ergonomics, *Int. J. Environ. Res. Public Health*, 2020, **17**(10), 3554.

25 E. J. Markvicka, R. Tutika, M. D. Bartlett and C. Majidi, Soft electronic skin for multi-site damage detection and localization, *Adv. Funct. Mater.*, 2019, **29**(29), 1900160.

26 M. G. Mohammed and R. Kramer, All-printed flexible and stretchable electronics, *Adv. Mater.*, 2017, **29**(19), 1604965.

27 A. Lancaster and M. Keswani, Integrated circuit packaging review with an emphasis on 3d packaging, *Integration*, 2018, **60**, 204–212.

28 S. J. Woodman, D. S. Shah, M. Landesberg, A. Agrawala and R. Kramer-Bottiglio, Stretchable arduinos embedded in soft robots, *Science Robotics*, 2024, **9**(94), eadn6844.

29 S. Liu, D. S. Shah and R. Kramer-Bottiglio, Highly stretchable multilayer electronic circuits using biphasic gallium-indium, *Nat. Mater.*, 2021, **20**(6), 851–858.

30 P. A. Lopes, D. F. Fernandes, A. F. Silva, D. G. Marques, A. T. De Almeida, C. Majidi and M. Tavakoli, Bi-Phasic Ag-In-Ga-Embedded Elastomer Inks for Digitally Printed, Ultra-Stretchable, Multi-layer Electronics, *ACS Appl. Mater. Interfaces*, 2021, **13**, 14552–14561.

31 C. Zhang, Q. Yang, H. Li, Z. Luo, Y. Lu, J. Zhang, C. Li and F. Chen, 3d laser structuring of supermetalphobic microstructures inside elastomer for multilayer high-density interconnect soft electronics, *Int. J. Extreme Manuf.*, 2025, **7**(3), 035004.

32 J. Yoon, S. Y. Hong, Y. Lim, S.-J. Lee, G. Zi and J. S. Ha, Design and fabrication of novel stretchable device arrays on a deformable polymer substrate with embedded liquid-metal interconnections, *Adv. Mater.*, 2014, **26**(38), 6580–6586.

33 D. H. Ho, C. Hu, L. Li and M. D. Bartlett, Soft electronic vias and interconnects through rapid three-dimensional assembly of liquid metal microdroplets, *Nat. Electron.*, 2024, **7**(11), 1015–1024.

34 M. Tavakoli, P. Alhais Lopes, A. Hajalilou, A. F. Silva, M. Reis Carneiro, J. Carvalheiro, J. Marques Pereira and A. T. de Almeida, 3R Electronics: Scalable Fabrication of Resilient, Repairable, and Recyclable Soft-Matter Electronics, *Adv. Mater.*, 2022, **34**, 2203266.

35 A. Hajalilou, E. Parvini, T. A. Morgado, P. Alhais Lopes, M. E. Melo Jorge, M. Freitas and M. Tavakoli, Replacing the gallium oxide shell with conductive ag: Toward a printable and recyclable composite for highly stretchable electronics, electromagnetic shielding, and thermal interfaces, *ACS Appl. Mater. Interfaces*, 2024, **16**(44), 61157–61168.

36 Y. Peng, J. Dong, J. Sun, Y. Mao, Y. Zhang, J. Long, L. Li, C. Zhang, Y. Zhao, H. Lu, H.-L. Qian, X.-P. Yan, J. Zhao, F. Wang, Y. Huang and T. Liu, Multimodal health monitoring *via* a hierarchical and ultrastretchable all-in-one electronic textile, *Nano Energy*, 2023, **110**, 108374.

37 J. Yang, P. Nithyanandam, S. Kanetkar, K. Y. Kwon, J. Ma, S. Im, J.-H. Oh, M. Shamsi, M. Wilkins, M. Daniele, T.-I. Kim, H. N. Nguyen, V. K. Truong and M. D. Dickey, Liquid metal coated textiles with autonomous electrical healing and antibacterial properties, *Adv. Mater. Technol.*, 2023, **8**(14), 2202183.

38 C. Cao, H. Su, L. Ai, D. Lv, J. Gu, R. Li, D. Li, W. Zhang, M. Ge and X. Yao, Highly stable liquid metal-based electronic textiles by adaptive interfacial interactions, *Adv. Funct. Mater.*, 2024, **34**(49), 2409586.

39 R. A. Shveda, A. Rajappan, T. F. Yap, Z. Liu, M. D. Bell, B. Jumet, V. Sanchez and D. J. Preston, A wearable textile-based pneumatic energy harvesting system for assistive robotics, *Sci. Adv.*, 2022, **8**(34), eabo2418.

40 B. Jumet, Z. A. Zook, A. Yousaf, A. Rajappan, D. Xu, T. F. Yap, N. Fino, Z. Liu, M. K. O'Malley and D. J. Preston,

Fluidically programmed wearable haptic textiles, *Device*, 2023, **1**(3), 100059.
41 J. Kim, J. Fan, G. Petrossian, X. Zhou, P. Kateb, N. Gagnon-Lafrenais and F. Cicoira, Self-healing, stretchable and recyclable polyurethane-pedot:pss conductive blends, *Mater. Horiz.*, 2024, **11**, 3548–3560.
42 R. Liu, K. Xia, T. Yu, F. Gao, Q. Zhang, L. Zhu, Z. Ye, S. Yang, Y. Ma and J. Lu, Multifunctional smart fabrics with integration of self-cleaning, energy harvesting, and thermal management properties, *ACS Nano*, 2024, **18**(45), 31085–31097.
43 Z. Zhao, K. Xia, Y. Hou, Q. Zhang, Z. Ye and J. Lu, Designing flexible, smart and self-sustainable supercapacitors for portable/wearable electronics: from conductive polymers, *Chem. Soc. Rev.*, 2021, **50**(22), 12702–12743.
44 Y. Liang, P. Xiao, F. Ni, L. Zhang, T. Zhang, S. Wang, W. Zhou, W. Lu, S.-W. Kuo and T. Chen, Biomimetic underwater self-perceptive actuating soft system based on highly compliant, morphable and conductive sandwiched thin films, *Nano Energy*, 2021, **81**, 105617.
45 X. Qi, H. Zhao, L. Wang, F. Sun, X. Ye, X. Zhang, M. Tian and L. Qu, Underwater sensing and warming E-textiles with reversible liquid metal electronics, *Chem. Eng. J.*, 2022, **437**, 135382.
46 H. Pourkheyrollah, P. F. Shahandashti, A. Meimandi, A. Jahanshahi and H. Ghafoorifard, On Economically Viable Stretchable Washable Electronics Technology: Proof of Concept, in 2019 27th Iranian Conference on Electrical Engineering (ICEE), 285-289, IEEE, apr 2019.
47 J. T. Reeder, J. Choi, Y. Xue, P. Gutruf, J. Hanson, M. Liu, T. Ray, A. J. Bandodkar, R. Avila, W. Xia, S. Krishnan, S. Xu, K. Barnes, M. Pahnke, R. Ghaffari, Y. Huang and J. A. Rogers, Waterproof, electronics-enabled, epidermal microfluidic devices for sweat collection, biomarker analysis, and thermography in aquatic settings, *Sci. Adv.*, 2019, **5**, eaau6356.
48 S.-H. Lu, Y. Li and X. Wang, Soft, flexible conductivity sensors for ocean salinity monitoring, *J. Mater. Chem. B*, 2023, **11**, 7334–7343.
49 Y. Li, G. Wu, G. Song, S. H. Lu, Z. Wang, H. Sun, Y. Zhang and X. Wang, Soft, pressure-tolerant, flexible electronic sensors for sensing under harsh environments, *ACS Sens.*, 2022, **7**, 2400–2409.
50 S. Liu, D. Zhang, X. Fu, L. Mo, Q. Miao, R. Huang, X. Huang, W. Guo, Y. Li, Q. Zheng, G. Yang, K. Bai, B. Xie, Z. Yin and H. Wu, Tactile sensing for soft robotic manipulators in 50 mpa hydrostatic pressure environments, *Adv. Intell. Syst.*, 2023, **5**, 2300296.
51 E. J. Barron, E. T. Williams, B. T. Wilcox, D. H. Ho and M. D. Bartlett, Liquid metal-elastomer composites for water-resilient soft electronics, *J. Polym. Sci.*, 2023, **62**(16), 1–12.
52 C.-h Kim, J. Kim, J. Fan, M. Wang and F. Cicoira, Recyclable printed liquid metal composite for underwater stretchable electronics, *Small Sci.*, 2025, **5**(5), 2400553.
53 I. You, M. Kong and U. Jeong, Block Copolymer Elastomers for Stretchable Electronics, *Acc. Chem. Res.*, 2019, **52**, 63–72.
54 C. Creton, G. Hu, F. Deplace, L. Morgret and K. R. Shull, Large-strain mechanical behavior of model block copolymer adhesives, *Macromolecules*, 2009, **42**, 7605–7615.
55 D. J. Kim, H. J. Kim and G. H. Yoon, Effects of blending and coating methods on the performance of SIS (styrene-isoprene-styrene)-based pressure-sensitive adhesives, *J. Adhes. Sci. Technol.*, 2004, **18**(15–16), 1783–1797.
56 D. J. Kim, H. J. Kim and G. H. Yoon, Shear creep resistance of styrene–isoprene–styrene (SIS)-based hot-melt pressure-sensitive adhesives, *J. Appl. Polym. Sci.*, 2006, **100**, 825–831.
57 D. J. Kim, W. J. Kim and G. H. Yoon, Tack and fracture energy of tackified SIS (styrene-isoprene-styrene)-based hot-melt pressure sensitive adhesives (HMPSAs), *J. Adhes. Sci. Technol.*, 2006, **20**(12), 1367–1381.
58 F. X. Gibert, G. Marin, C. Derail, A. Allal and J. Lechat, Rheological properties of hot melt pressure-sensitive adhesives based on styrene - Isoprene copolymers. Part 1: A rheological model for [SIS-SI] formulations, *J. Adhes.*, 2003, **79**, 825–852.
59 J. Xue, J. Wang, H. Huang, M. Wang, Y. Zhang and L. Zhang, Feasibility of processing hot-melt pressure-sensitive adhesive (Hmpsa) with solvent in the lab, *Processes*, 2021, **9**, 1608.
60 J. Widmaier and G. Meyer, Molecular-Weight Dependence of the Glass Transition Temperatures of Rigid SIS Triblock Copolymers Studied by DSC, *J. Therm. Anal.*, 1982, **23**, 193–199.
61 M. D. Bartlett, S. W. Case, A. J. Kinloch and D. A. Dillard, Peel tests for quantifying adhesion and toughness: A review, *Prog. Mater. Sci.*, 2023, **137**, 101086.
62 D. Zhalmuratova, T. G. La, K. T. T. Yu, A. R. Szojka, S. H. Andrews, A. B. Adesida, C. I. Kim, D. S. Nobes, D. H. Freed and H. J. Chung, Mimicking ''j-Shaped'' and Anisotropic Stress-Strain Behavior of Human and Porcine Aorta by Fabric-Reinforced Elastomer Composites, *ACS Appl. Mater. Interfaces*, 2019, **11**, 33323–33335.
63 X. Xu, G. Wang, H. Yan and X. Yao, Constitutive relationship of fabric rubber composites and its application, *Compos. Struct.*, 2023, **304**, 116302.
64 D. Zhalmuratova and H. J. Chung, Reinforced Gels and Elastomers for Biomedical and Soft Robotics Applications, *ACS Appl. Polym. Mater.*, 2020, **2**, 1073–1091.
65 P. Lall, H. Jang, B. Leever and S. Miller, Folding-Reliability of Flexible Electronics in Wearable Applications, ASME 2019 International Technical Conference and Exhibition on Packaging and Integration of Electronic and Photonic Microsystems, InterPACK 2019, dec 2019.
66 T. Chalklen, M. Smith and S. Kar-Narayan, Improved fatigue resistance in transfer-printed flexible circuits embedded in polymer substrates with low melting temperatures, *Flexible Printed Electron.*, 2023, **8**, 025014.
67 S.-M. Yi, I.-S. Choi, B.-J. Kim and Y.-C. Joo, Reliability Issues and Solutions in Flexible Electronics Under Mechanical Fatigue, *Electron. Mater. Lett.*, 2018, **14**, 387–404.
68 H.-Y. Lee, S.-M. Yi, J.-H. Lee, H.-S. Lee, S. Hyun and Y.-C. Joo, Effects of bending fatigue on the electrical resistance in metallic films on flexible substrates, *Met. Mater. Int.*, 2010, **16**, 947–951.
69 B.-J. Kim, M.-H. Jeong, H. Sung-Hwan, H.-Y. Lee, S.-W. Lee, K.-D. Chun, Y.-B. Park and Y.-C. Joo, Relationship between

tensile characteristics and fatigue failure by folding or bending in cu foil on flexible substrate, *J. Microelectron. Packag. Soc.*, 2011, **18**, 55–59.

70 F. Bossuyt, J. Guenther, T. Löher, M. Seckel, T. Sterken and J. de Vries, Cyclic endurance reliability of stretchable electronic substrates, *Microelectron. Reliab.*, 2011, **51**, 628–635.

71 A. K. Persons, J. E. Ball, C. Freeman, D. M. Macias, C. L. Simpson, B. K. Smith and R. V. Burch, Fatigue testing of wearable sensing technologies: Issues and opportunities, *Materials*, 2021, **14**, 4070.

72 G. Li, X. Chen, F. Zhou, Y. Liang, Y. Xiao, X. Cao, Z. Zhang, M. Zhang, B. Wu and S. Yin, *et al.*, Self-powered soft robot in the mariana trench, *Nature*, 2021, **591**(7848), 66–71.